Design Optimization of Equiangular Spiral Photonic Crystal Fiber for Large Negative Flat Dispersion and High Birefringence

Md. Asiful Islam and M. Shah Alam, *Senior Member, IEEE*

***Abstract*—The design of a residual dispersion compensating fiber in an equiangular spiral photonic crystal fiber (ES-PCF) structure is presented in the wavelength range 1350–1650 nm. A step-by-step design optimization is demonstrated and a maximum optimized value of average dispersion -393 ps/nm km with a flattened dispersion profile with a very high birefringence is reported. It has been found that for the ES-PCF, a very high birefringence of 0.0278 at the wavelength 1550 nm can be obtained by employing an elliptical air hole as defect in the core region. An efficient full-vectorial finite-element method with vector edge element is employed in this study. The proposed ES-PCF can be an excellent candidate to be used in a wavelength-division-multiplexing optical fiber transmission system for residual chromatic dispersion compensation as well as maintaining single polarization.**

***Index Terms*—Birefringence, dispersion compensating fiber (DCF), polarization maintaining fiber, residual dispersion.**

I. Introduction

PHOTONIC CRYSTAL FIBERS (PCFs) have created significant attention in the field of optical fiber communication in recent years. Index guiding PCFs [1], [2] have a microscopic array of air channels running down their length that make a low-index cladding around the undoped solid silica core. Among the arrangements of the cladding air holes, the hexagonal lattice arrangement is the most common where the air holes have a fixed hole-to-hole spacing. Such a cladding arrangement in PCFs offers many useful properties like tailoring of chromatic dispersion, low confinement loss, etc., than those of conventional optical fibers [3]. Apart from hexagonal lattice, other air hole arrangements are also proposed and reported for many useful properties [4], [5]. Very recently, an equiangular spiral photonic crystal fiber (ES-PCF) for small effective mode area with a high nonlinearity and ultraflattened dispersion profile has also been reported [6]. Further investigation on ES-PCF was also carried out to obtain two zero dispersion wavelengths to find its possibility to be used for supercontinuum generation in the visible region [6], [7]. Thus, it is expected that unique and useful properties may be obtained by tailoring the ES-PCF design for fiber-optic communication system.

A long-haul optical fiber transmission system usually has a small but nonzero flattened dispersion characteristics around 10 ps/nm km [8]. So, a dispersion management scheme should be there to nullify the accumulated residual dispersion over a long distance in the system. For this purpose, a fiber having a large negative dispersion called dispersion compensating fiber (DCF) has to be introduced as a part of the communication system [9]–[11]. Flat negative dispersion of about -98.3 ps/nm km with absolute dispersion variation of 1.1 ps/nm km was reported over $S+C+L$ wavelength bands in [11]. The design in [9] exhibits ultraflattened negative dispersion over $S+C+L+U$ wavelength bands and average dispersion of about -179 ps/nm km with an absolute dispersion variation of 2.1 ps/nm km over 1480–1675 nm (195 nm bandwidth). More recently, a genetic algorithm-based optimization technique has been reported in [10] to achieve a flattened negative dispersion over $\mathrm{E}+S+C+L+U$ wavelength bands with an average dispersion of -212 ps/nm km with a dispersion variation of 11 ps/nm km by employing a small Ge-doped core at the center. All these analyses are done on the microstructured fiber with hexagonal-lattice of air holes. But, the polarization issue was not considered anywhere. However, very recently, a large negative average dispersion of about -227 ps/nm km over the wavelength range 1350–1675 nm has been reported by the authors for an ES-PCF structure with a dispersion variation of about 10 ps/nm km [12], where one elliptical air hole is introduced in the core.

In this paper, the dispersion profile and birefringence of the ES-PCF are investigated by introducing more than one air holes in the core region to obtain a dispersion profile even flatter than that of our previous work [12] with less dispersion variation over the wavelength range 1350–1650 nm. Dispersion profiles having average dispersion of about -293.5 and -393 ps/nm km over the wavelength range of interest have been reported here with dispersion variation of only 8.6 and 10.4 ps/nm km, respectively. Also, a further investigation has been carried out to obtain a higher birefringence in the order of 10^{-2} over the wavelength range 1350–1650 nm (0.0278 at 1550 nm.). Furthermore, the higher order modes (HOMs) of this ES-PCF are suppressed by introducing a secondary annular core in the outer cladding region.

II. ES-PCF Design

The structure of the proposed residual dispersion compensating fiber (RDCF), which is basically an ES-PCF having air

Manuscript received June 26, 2012; revised September 02, 2012 and September 20, 2012; accepted September 24, 2012. Date of publication October 03, 2012; date of current version December 05, 2012.

The authors are with the Department of Electrical and Electronic Engineering, Bangladesh University of Engineering and Technology, Dhaka 1000, Bangladesh (e-mail: maislam@eee.buet.ac.bd; shalam@eee.buet.ac.bd).

Color versions of one or more of the figures in this paper are available online at http://ieeexplore.ieee.org.

Digital Object Identifier 10.1109/JLT.2012.2222349

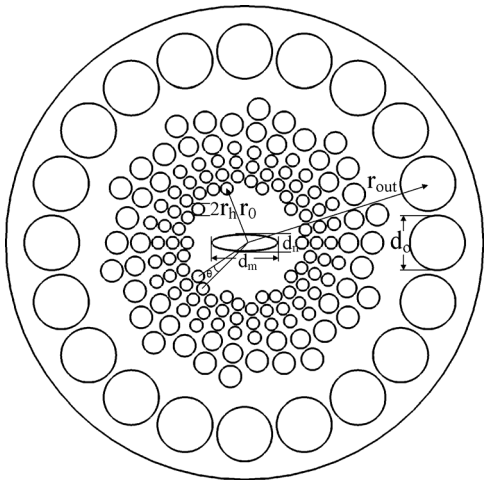

Fig. 1. Geometrical model of the proposed RDCF, where $r_o = \text{the}$ radius of the first air hole ring in the cladding, $\theta = \text{angular}$ increment of each air hole in spiral arms, and $2r_h = \text{the}$ diameter of the air holes in the first nine rings.

hole arrangement in silica background, is shown in Fig. 1. There are N_r air holes in each ring, the first ring has a radius of r_o, and the radii of the rings in the same arm increase by geometric progression. There are N circular air holes in each arm. The first seven of them have a radius of r_h. The radii of the subsequent air holes in the same arm are increased gradually. The angular position of each air hole in an arm is increased by θ than the previous one. Here, d_m and d_n are major and minor axes of the elliptical air hole at the center of the core, respectively.

In this design process, a full-vectorial finite-element method [13] has been used to characterize the proposed ES-PCF. An anisotropic perfectly matched layer was used to accurately account for the confinement losses. Chromatic dispersion caused by the combined effects of material and waveguide dispersions in an optical fiber can be calculated by the formula

$$D = -\frac{\lambda}{c}\frac{\partial^2(\mathrm{Re}(n_{\mathrm{eff}}))}{\partial\lambda^2} \tag{1}$$

where λ is the wavelength, c is the velocity of light, n_{eff} is the effective refractive index of the fundamental mode, and $\mathrm{Re}(\cdot)$ indicates the real part. The birefringence is determined by taking the difference of the real parts of the effective indices of two fundamental orthogonal polarization modes (slow and fast axis modes) [14]

$$\mathrm{B} = |n_{\mathrm{eff}}^x - n_{\mathrm{eff}}^y|\,. \tag{2}$$

As will be shown later, the PCF is birefringent due to the presence of central elliptical air hole and also the large negative flat dispersion profile is obtained by optimizing this air hole. So, the high birefringence can be exploited to achieve a single polarization dispersion compensating PCF. Here, the dispersion properties are shown for the fundamental slow axis mode. Also, the material dispersion is taken into account here by using the Sellmeier equation [15] to obtain the refractive index of silica at different wavelengths. In most cases, the following structural parameters are kept unchanged unless otherwise stated: $N_r = 10, N = 16, r_o = 1.4\ \mu$m, $\theta = 12°$, and $r_h = 0.148\ \mu$m. As shown in Fig. 1, a secondary annular core is introduced in the outer cladding by employing an air hole ring having radial distance from the center, $r_{\mathrm{out}} = 5.88\ \mu$m resulting in a dual core ES-PCF. The diameter of the air holes of this ring is $d_0 = 1.68\ \mu$m.

It is seen that the effective index of the propagating fundamental modes (slow and fast axis modes) lies between the effective cladding index and the effective core index. As the proposed PCF has a very high birefringence, the effective index of the fundamental fast axis mode is much lower than the effective core index of the fiber as compared to the effective index of the fundamental slow axis mode. The values of r_{out} and d_0 are so optimized that the resulting secondary core modes occur as degenerate modes with the HOMs of the central core and the fundamental fast axis mode of the central core. Because of this index matching, coupling of energy occurs, and thus, the central HOMs and the fundamental fast axis mode become very lossy over the entire wavelength range of interest [16]. It is observed that these modes have confinement loss more than 1 dB/m and can be effectively suppressed to realize the single-mode (SM) condition in ES-PCF. It should be noted here that single modedness in H-PCF has been realized similarly in [17].

The proposed PCF can be fabricated using the sol-gel technique which has already been used for fabricating PCF of various irregular structures [18]. In this method, the air hole size, shape, and spacing may all be adjusted independently. Photonic bandgap structures having very small dimensions have also been fabricated using this technique [19].

III. Results and Discussion

The dispersion and birefringence properties of the ES-PCF structure with one circular air hole ($d_m = d_n$) in the center of the core are shown in Figs. 2 and 3, respectively. In Fig. 2, we can see that the dispersion becomes more negative with the introduction of air hole in the core, and the value increases further with the increase of its radius. Here, the blue line shows a flattened profile of average dispersion about 10 ps/nm km over 1350–1650 nm wavelength bands when the diameter of the central hole, $d_m = d_n = 0.17\ \mu$m. For $d_m = d_n = 1.02\ \mu$m, the average dispersion is -300 ps/nm km with a flat profile having a dispersion variation of 35 ps/nm km around the mean value. This is a large negative value as compared to those reported in [9]–[12], but the flatness should be improved.

We can also notice from Fig. 2 that the more negative the dispersion goes, the less flat its profile becomes. A tradeoff has to be made between the flatness and higher negative values of dispersion. From Fig. 3, we can see that the birefringence of the ES-PCF increases after introducing a circular air hole in the core. The birefringence also increases with the increase of diameter of this air hole. It is perhaps due to the fact that the symmetry of the structure is disturbed more due to the increase in diameter of the central air hole.

Now, we consider a single elliptical air hole in the core and show the dispersion and birefringence properties in Figs. 4 and 5, respectively. Here, the effect of ellipticity (defined as the ratio of major axis length to minor axis length) on dispersion and birefringence has been demonstrated. In Fig. 4, we can see that the dispersion becomes more negative for lower ellipticity that results in larger size of the air hole as expected [20]. Here, for

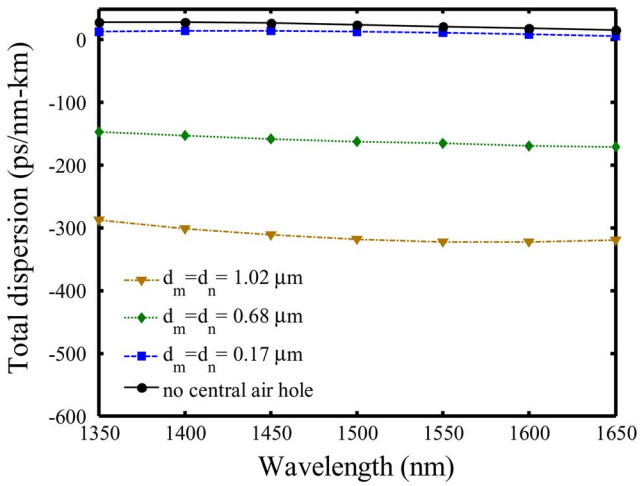

Fig. 2. Total dispersion versus wavelength for circular air hole of different radius in the core.

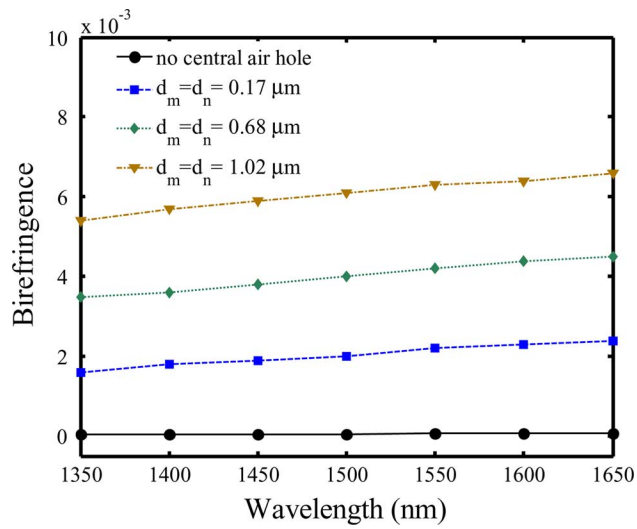

Fig. 3. Birefringence versus wavelength for circular air hole of different radius in the core.

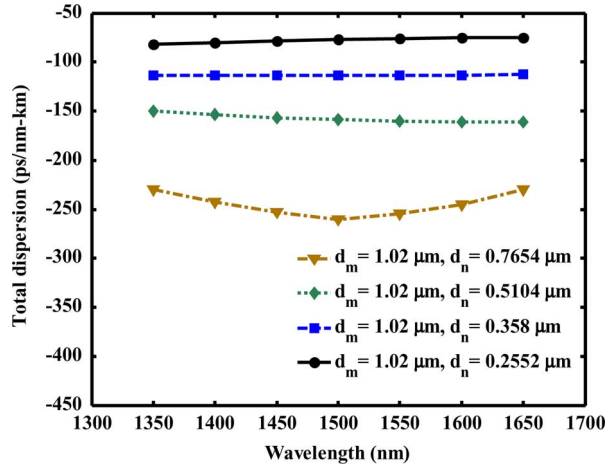

Fig. 4. Total dispersion versus wavelength for one elliptical air hole of different ellipticity in the core.

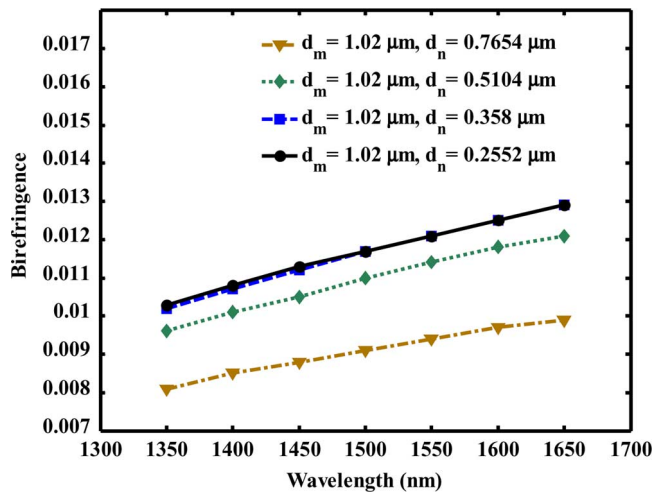

Fig. 5. Birefringence versus wavelength for one elliptical air hole of different ellipticity in the core.

$d_m = 1.02$ μm and $d_n = 0.7654$ μm, the gray line with triangular marker shows an average dispersion of -245 ps/nm km over 1350–1650 nm wavelength bands with a dispersion variation of about 30 ps/nm km. This value is less negative but slightly flatter than that shown in Fig. 2, where the dispersion variation is about 34.6 ps/nm km for a circular central air hole with $d_m = d_n = 1.02$ μm, although the flatness should be improved more to be used effectively as a DCF. A more flat profile with less negative dispersion values has been achieved by optimizing the structural parameters for the same structure as reported in [12]. It can be seen in Fig. 4 that an ultraflattened dispersion profile can be obtained when $d_n = 0.358$ μm as shown by the blue line with square markers. In this case, an average dispersion of -113 ps/nm km over 1350–1650 nm wavelength bands with a dispersion variation of only ~ 0.5 ps/nm km between ~ 13.25 and ~ 12.75 ps/nm km can be obtained.

From Fig. 5, we can see that the birefringence becomes higher with the increase in ellipticity, although the dispersion becomes less negative. This is because higher asymmetry is encountered by the field with the increased ellipticity of the central air hole. If we optimize the structural parameters to obtain a higher birefringence, we get even higher value of birefringence over the wavelength bands of interest. The birefringence increases with the decrease of r_0 when other dimensions are unchanged, as shown in Fig. 6. The highest value of birefringence is found to be 0.0278 at the wavelength of 1550 nm for the parameters $d_m = 1.3089$ μm, $d_n = 0.3272$ μm, $r_0 = 0.9696$ μm, and $r_h = 0.115$ μm shown in Fig. 6. This birefringence is very high, even higher than the values reported in [21] and [22]. However, this structure shows an average dispersion of -113 ps/nm km with a variation of about 14 ps/nm km over the wavelength range 1350–1650 nm.

We have observed that large negative dispersion with high birefringence can be achieved with even one elliptical air hole in the core by increasing the size of the hole. But, as the dispersion gets more negative, it becomes less flat. Now, we introduce more air holes in the core region, as shown in Fig. 7, and study dispersion and birefringence properties for each case separately to obtain large negative as well as flat dispersion profile with high birefringence. In Fig. 8, the dispersion properties are shown for

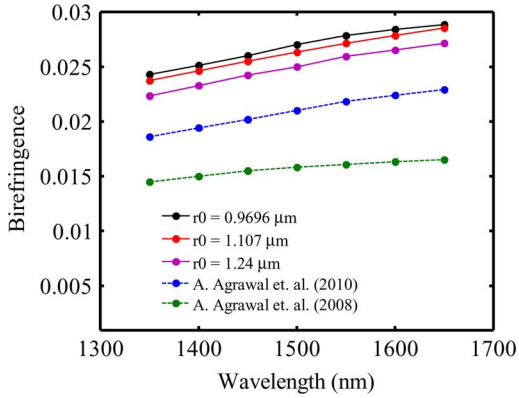

Fig. 6. Birefringence versus wavelength as a function of r_o.

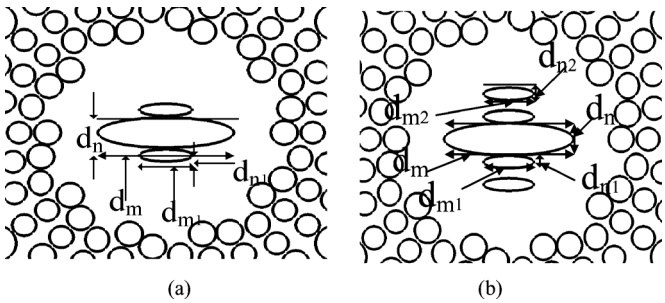

Fig. 7. Different number of elliptical air holes in the core with their dimensions, in (a) three air holes, (b) five air holes, and (c) seven air holes in the core.

the structure of Fig. 7(a), where for additional holes, the major and minor axes are d_{m1} and d_{n1}, respectively. The size of central air hole is kept fixed at $d_m = 1.02$ μm, $d_n = 0.2552$ μm because at values greater than these, the modal effective area becomes very small resulting in high splice loss with an standard single-mode fiber (SMF). The sizes of the additional two elliptical air holes are varied keeping their ellipticity (d_{m1}/d_{n1}) fixed at 4 because birefringence is seen to be maximum around this value. It can be seen that the dispersion gets more negative with the introduction of two more elliptical air holes. Also, as the size of these extra air holes increases, the dispersion becomes more negative. The gray line with triangular marker in Fig. 8 has an average dispersion of about -340 ps/nm km with a dispersion variation of $\sim$16 ps/nm km over the wavelength bands of interest, and this value is far more negative than those reported in [7]–[9] though the curve is slightly less flat. However, for these structures, the birefringence remains in the order of 10^{-2} and is seen to be decreasing after introducing the two additional air holes in the core and also with the increase of the size of these two air holes, as shown in Fig. 9.

With the intuition of obtaining a large negative as well as flat dispersion profile over the wavelength band of interest, we consider another structure shown in Fig. 7(b). The additional two air holes have major and minor axes of d_{m2} and d_{n2}, respectively. The sizes of previous three air holes are kept fixed at $d_m = 1.02$ μm, $d_n = 0.2552$ μm, $d_{m1} = 0.567$ μm, and $d_{n1} = 0.1418$ μm, and the sizes of the newly introduced two are varied keeping their ellipticity fixed at 4 for the same reason stated previously. From Fig. 10, we can see that the dispersion gets more negative after employing those extra two air holes

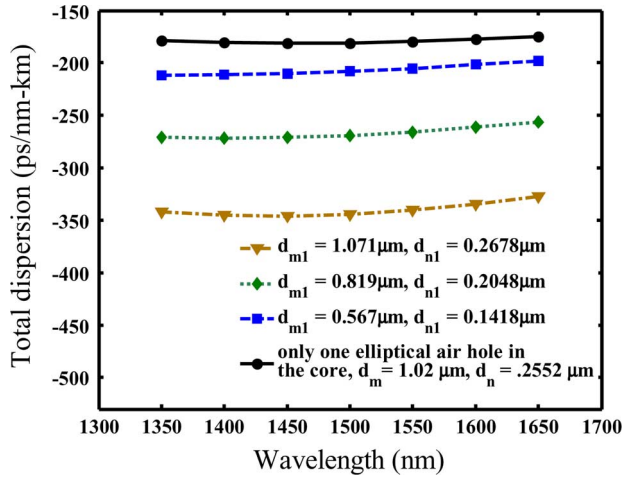

Fig. 8. Total dispersion versus wavelength for additional two elliptical air holes of different size in the core.

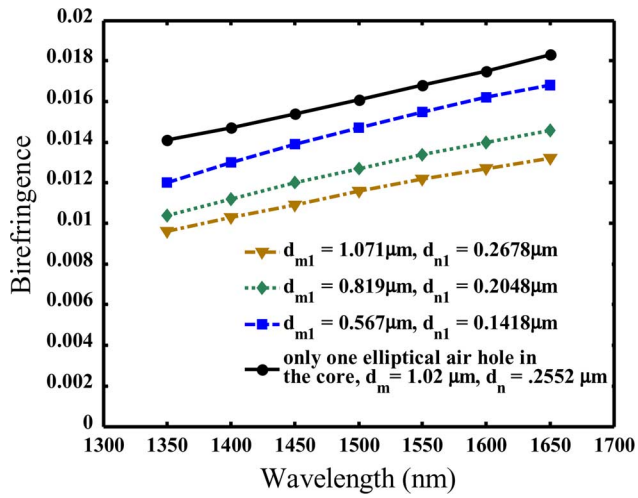

Fig. 9. Birefringence versus wavelength for additional two elliptical air hole of different size in the core.

and becomes even more negative for increased size. The curves shown by the gray line with triangular marker has an average dispersion of about -396 ps/nm km with a dispersion variation of only 10.4 ps/nm km and the green line with diamond marker has an average dispersion of about -296 ps/nm km with a dispersion variation of only around 8.6 ps/nm km over the wavelength bands of interests are even far more negative than those reported in [9]–[11] and also more flat or flat almost as like as that of [10]. However, the birefringence remains between the orders of 10^{-3}–10^{-2} for these structural parameters and is seen to be decreasing when these two additional air holes are introduced in the core and also with the increase of the size of these two air holes, as shown in Fig. 11. It is observed and also can be deduced from Figs. 3, 5, 9, and 11 that the birefringence is maximum for the structure of Fig. 1 with hole ellipticity around 4 and it decreases with the introduction of more holes in the core resulting in structures of Fig. 7(a)–(b). It is observed that the introduction of more elliptical air holes in the core of structure in Fig. 7(b) does not result in significant improvement in birefringence and in the dispersion profile to be used for dispersion

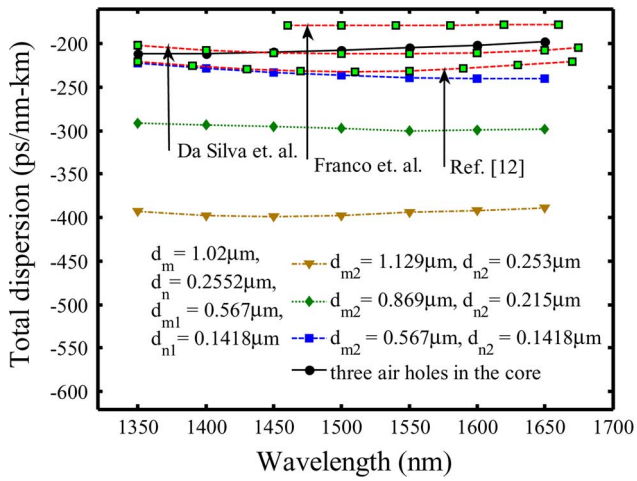

Fig. 10. Total dispersion versus wavelength for additional four elliptical air holes of different size in the core.

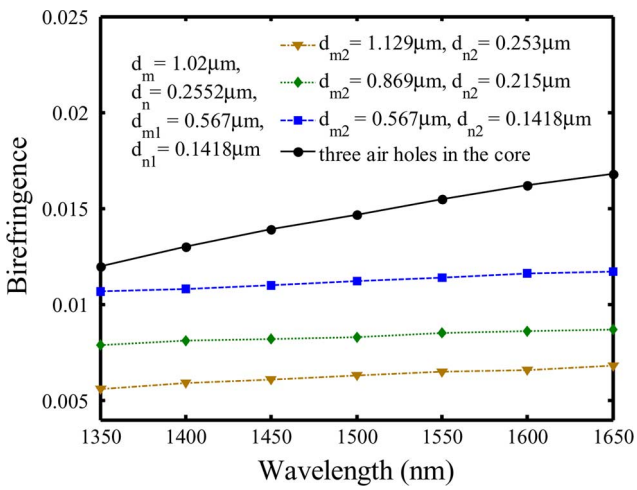

Fig. 11. Birefringence versus wavelength for additional four elliptical air hole of different size in the core.

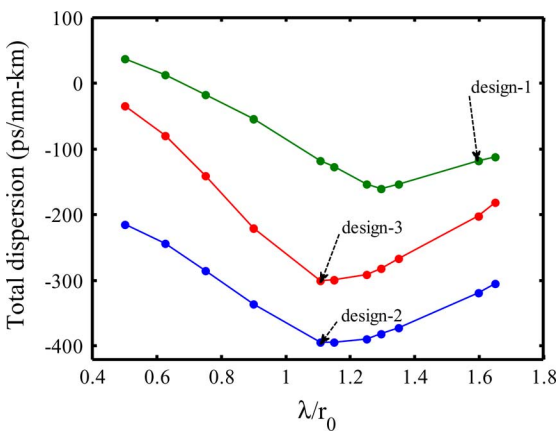

Fig. 12. Total dispersion as a function of r_0.

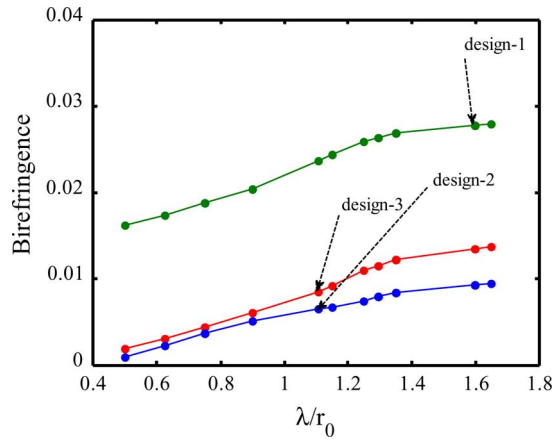

Fig. 13. Birefringence as a function of r_0.

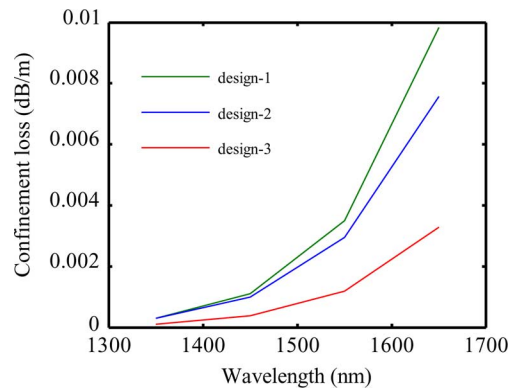

Fig. 14. Confinement loss versus wavelength of the fundamental mode for the proposed ES-PCF designs.

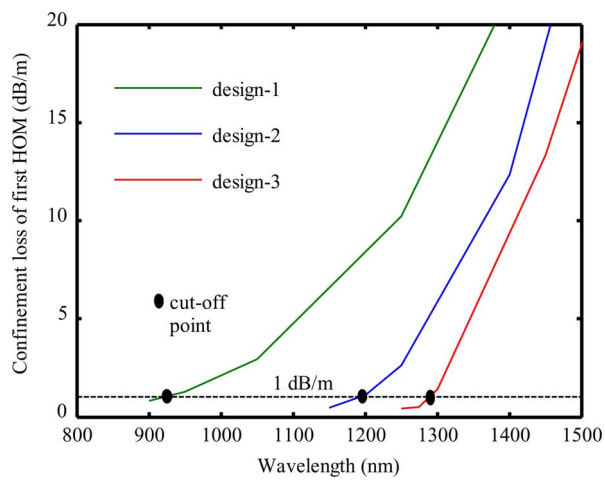

Fig. 15. Confinement loss of the first HOM versus wavelength for the proposed ES-PCF designs.

compensation. So, the analysis is shown for a maximum of five air holes in the core.

In Table I, the optimized designs of the proposed ES-PCFs are summarized. The main focus of design 1 is to obtain an ES-PCF with high birefringence, while the main focus of the other two designs, designs 2 and 3, is to obtain ES-PCFs with flat large negative dispersion profile over the wavelength range 1350–1650 nm. Design 2, however, provides more negative dispersion with less flatness than design 3.

The hole sizes may deviate from the optimized values during fabrication of the ES-PCF. As the dispersion and the birefrin-

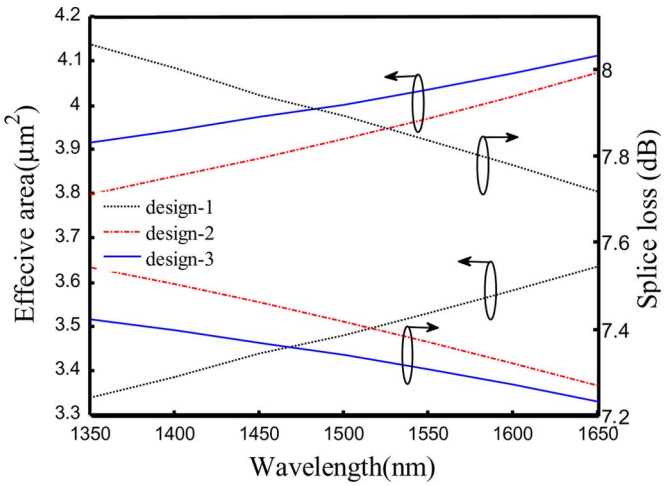

Fig. 16. Effective area and splice loss versus wavelength for the proposed ES-PCF designs.

TABLE I
SUMMARY OF THE PROPOSED ES-PCF DESIGNS

Design No.	Structural parameters	Dispersion and Birefringence properties
1	r_0= 0.9696 μm, r_h= 0.115 μm d_m= 1.3089 μm and d_n= 0.3272 μm	B = 0.0278 at λ = 1.55 μm, D = −115 ps/nm-km, ΔD = 14 ps/nm-km over λ = 1.35 to 1.65 μm
2	r_0= 1.4 μm, r_h= 0.148 μm, d_m= 1.02 μm, d_n= 0.2552 μm, d_{m1}= 0.567 μm, d_{n1}= 0.1418 μm, d_{m2}= 1.129 μm and d_{n2}= 0.253 μm	B = 0.0065 at λ = 1.55 μm, D = −393 ps/nm-km, ΔD = 10.4 ps/nm-km over λ = 1.35 to 1.65 μm
3	r_0= 1.4 μm, r_h= 0.148 μm, d_m= 1.02 μm, d_n= 0.2552 μm, d_{m1}= 0.567 μm, d_{n1}= 0.1418 μm, d_{m2}= 0.869 μm and d_{n2}= 0.215 μm	B = 0.0085 at λ = 1.55 μm, D = −293.5 ps/nm-km, ΔD = 8.6 ps/nm-km over λ = 1.35 to 1.65 μm

D = Average dispersion, ΔD = Dispersion variation

gence are very sensitive to the size of the central elliptical air hole, it has been found by simulation that birefringence changes about 10% for design 1 and dispersion changes up to 4% for designs 2 and 3 with a deviation of 5% in the central elliptical air hole size. However, these changes are not very significant.

In Figs. 12 and 13, the total dispersion and the birefringence, respectively, are shown as functions of r_0 at $\lambda = 1550$ nm. Here, in these figures, by varying r_0, the whole structure is scaled up or down. In Fig. 12, it can be seen that the minima of the total dispersion curves of blue and red color occur at those r_0 corresponding to designs 2 and 3, respectively, as expected. As design 1 is optimized to obtain a very high birefringence and the focus was not on obtaining a large negative dispersion, the minima of the green line in Fig. 12 is not at the r_0 corresponding to design 1. In Fig. 13, one could expect that the maxima of the green curve should occur at the r_0 corresponding to design 1. But, the maxima occurs for a value of r_0 which is obviously smaller than that of design 1.

This implies that higher birefringence can be achieved for lower r_0 values than the optimized one. But for r_0 lower than 0.9696 μm (design 1), the confinement loss becomes very high, as is evident from Fig. 14, where the confinement losses of the optimized designs are shown as a function of λ. The confinement loss can be calculated from the imaginary part of the complex effective index [20]

$$\text{Confinement Loss} = \frac{40\pi}{\ln(10)\lambda}\text{Im}(n_{\text{eff}}) \times 10^3 \qquad (3)$$

where $\text{Im}(n_{\text{eff}})$ is the imaginary part of n_{eff}. The other two designs, designs 2 and 3, are not optimized to obtain the highest birefringence rather they are optimized to obtain very large negative dispersion over the wavelength bands of interest. So, it is not unexpected that the maxima of the blue and red curves do not occur at those r_0 corresponding to designs 2 and 3, respectively. Here, all the ES-PCF designs are optimized so that the confinement loss of the fundamental mode lies within an acceptable limit of 0.01 dB/m over the entire wavelength range of interest. As shown in Fig. 14, the confinement loss increases with the decrease of structural dimensions. The confinement loss is the highest for design 1 because it has the lowest r_0 among the three designs. Also, design 2 has higher confinement loss than that of design 3. This is because the effective core index is lower in design 2 as it has elliptical air holes of larger size than those of design 3 resulting in reduced difference between the effective core index and effective cladding index. It is observed that confinement loss for all the designs increases if the number of air hole rings N in the cladding is decreased as expected. For this reason, a large number of $N = 16$ has to be employed to obtain confinement losses within the limit 0.01 dB/m over the entire wavelength range of interest.

Here, the single modedness of the ES-PCF is another important issue. We defined the SM operation of the ES-PCF in a way that the confinement loss of the first HOM should be greater than 1 dB/m [17]. Also, the confinement losses of the fundamental modes are about 1.15×10^4, 1.25×10^4, and 2.1×10^4 times lower than those of the first HOMs of the designs 1, 2, and 3, respectively, at 1.55 μm ensuring SM operation. One can see from Fig. 15 that the first HOMs have cutoff wavelengths around 925, 1195, and 1290 nm for designs 1, 2, and 3, respectively, which are well below the wavelength range of interest (1350–1650 nm).

The issue of splice loss becomes very critical when the PCF has to be jointed with a conventional SMF in a communication link for residual dispersion compensation and maintaining polarization. The splice loss due to mode field diameter (MFD) mismatch can be calculated from MFDs of two fibers using [23]

$$\text{Splice Loss [dB]} = 20\log\left[\frac{1}{2}\left(\frac{\text{MFD1}}{\text{MFD2}} + \frac{\text{MFD2}}{\text{MFD1}}\right)\right] \qquad (4)$$

where MFD1 and MFD2 are the MFDs of the two fibers. Splice loss depends mostly on the difference of MFDs of the two fibers of interest. Thus, from (4), average splice loss for both directions can be calculated. The splice loss increases with the increase of difference between these two MFDs. The average MFD of a typical SMF is taken to be 10 μm [21]. The MFDs of the proposed ES-PCF designs are calculated from $A_{\text{eff}} = \pi w^2$, where A_{eff} is the effective modal area and w is the mode field radius which

is half of MFD. The A_{eff} of the ES-PCF is calculated from the following [24]:

$$A_{\text{eff}} = \frac{\iint \left(|E^2|dxdy\right)^2}{\iint |E^4|dxdy}. \quad (5)$$

The A_{eff} and average splice losses between a typical SMF and the ES-PCF designs as functions of wavelength are shown in Fig. 16. Though the splice losses shown in Fig. 16 are high, they can be minimized by the technique proposed in [25]. This loss will also be reduced if an SMF to be spliced with the ES-PCF is used having MFD less than 10 μm.

IV. Conclusion

In this paper, ES-PCF is investigated as a polarization maintaining RDCF in the telecommunication wavelength bands. It is numerically shown to exhibit an average dispersion of -293.5 and -393 ps/nm km for two different designs with dispersion variation of only 8.6 and 10.4 ps/nm km, respectively. To our knowledge, this dispersion profile is more negative than the RDCFs reported earlier. Another unique feature of these designs is their high birefringence along with the property of dispersion compensation. An optimized structure exhibits a birefringence as high as 0.0278. The structural dependence as presented in the paper also shows that large negative and flattened dispersion and high birefringence can be obtained over a wide wavelength range, and this structure can be considered to be robust with respect to small variations in structural parameters that are unavoidable during fabrication. The dual characteristics of dispersion compensation and high birefringence make this fiber a promising candidate in its application in the fiber-optic communication link in the telecommunication window.

References

[1] J. C. Knight, "Photonic crystal fibres," *Nature*, vol. 424, no. 6950, pp. 847–851, Aug. 2003.

[2] P. Russell, "Photonic crystal fibers," *Science*, vol. 299, no. 5605, pp. 358–362, Jan. 2003.

[3] J. C. Knight, T. A. Birks, P. St. J. Russell, and D. M. Atkin, "All-silica single-mode optical fibre with photonic crystal cladding," *Opt. Lett.*, vol. 21, pp. 1547–1549, 1996.

[4] S. M. A. Razzak and Y. Namihira, "Proposal for highly nonlinear dispersion flattened octagonal photonic crystal fibers," *IEEE Photon. Technol. Lett.*, vol. 20, no. 4, pp. 249–251, Feb. 2008.

[5] A. Agrawal, N. Kejalakshmy, J. Chen, B. M. A. Rahman, and K. T. V. Grattan, "Soft glass equiangular spiral photonic crystal fiber for supercontinuum generation," *IEEE Photon. Technol. Lett.*, vol. 21, no. 22, pp. 1722–1724, Nov. 2009.

[6] M. N. Hossain, M. S. Alam, D. M. N. Hasan, and K. M. Mohsin, "A highly nonlinear spiral photonic crystal fiber for tailoring two zero dispersion wavelengths in the visible region," *Photon. Lett. Poland*, vol. 2, pp. 143–145, 2010.

[7] M. N. Hossain, M. S. Alam, D. M. N. Hasan, and K. M. Mohsin, "Design of a spiral silica photonic crystal fiber for nonlinear applications in visible region," *Opt. Eng.*, vol. 50, no. 7, p. 070503, Jul. 2011.

[8] G. P. Agrawal, *Fiber-Optic Communication Systems*, 3rd ed. New York: Wiley, 2002, pp. 15–64.

[9] M. A. R. Franco, V. A. Serrão, and F. Sircilli, "Microstructured optical fiber for residual dispersion compensation over $S+C+L+U$ wavelength bands," *IEEE Photon. Technol. Lett.*, vol. 20, no. 9, pp. 751–753, May 2008.

[10] J. P. da Silva, D. S. Bezerra, V. F. R. Esquerre, I. E. da Fonseca, and H. E. H. Figueroa, "Ge-doped defect-core microstructured fiber design by genetic algorithm for residual dispersion compensation," *IEEE Photon. Technol. Lett.*, vol. 22, no. 18, pp. 1337–1339, Sep. 2010.

[11] S. K. Varshney, N. J. Florous, K. Saitoh, M. Koshiba, and T. Fujisawa, "Numerical investigation and optimization of a photonic crystal fiber for simultaneous dispersion compensation over $S+C+L$ wavelength bands," *Opt. Commun.*, vol. 274, pp. 74–79, 2007.

[12] M. A. Islam and M. S. Alam, "Design of a polarization maintaining equiangular spiral photonic crystal fiber for residual dispersion compensation over *E+S+C+L+U* wavelength bands," *IEEE Photon. Technol. Lett.*, vol. 24, no. 11, pp. 930–932, Jun. 2012.

[13] COMSOL Multiphysics version 3.4 2007.

[14] Y. Yue, G. Kai, Z. Wang, T. Sun, L. Jin, Y. Lu, C. Zhang, J. Liu, Y. Li, Y. Liu, S. Yuan, and X. Dong, "Highly birefringent elliptic-hole photonic crystal fibre with squeezed hexagonal lattice," *Opt. Lett.*, vol. 32, pp. 469–471, 2007.

[15] G. Renversez, B. Kuhlmey, and R. McPhedran, "Dispersion management with microstructured optical fibers: Ultraflattened chromatic dispersion with low losses," *Opt. Lett.*, vol. 28, pp. 989–991, 2003.

[16] J. Fini, "Design of solid and microstructure fibers for suppression of higher order modes," *Opt. Exp.*, vol. 13, no. 9, pp. 3477–3490, 2005.

[17] T. Matsui, T. Sakamoto, K. Tsujikawa, S. Tomita, and M. Subokawa, "Single-mode photonic crystal fiber design with ultralarge effective area and low bending loss for ultrahigh-speed WDM transmission," *J. Lightw. Technol.*, vol. 29, no. 4, pp. 511–515, Feb. 2011.

[18] R. T. Bise and D. J. Trevor, "Sol-gel derived microstructured fibers: Fabrication and characterization," presented at the presented at the Opt. Fiber Commun. Conf., Washington, DC, Mar. 2005, Paper OWL6.

[19] R. M. Almeida and S. Portal, "Photonic band gap structures by sol-gel processing," *Curr. Opin. Solid State Mater. Sci.*, vol. 7, pp. 151–157, 2003.

[20] K. Saitoh, N. Florous, and M. Koshiba, "Ultra-flattened chromatic dispersion controllability using a defected core photonic crystal fiber with low confinement losses," *Opt. Exp.*, vol. 13, no. 21, pp. 8365–8371, 2005.

[21] A. Agrawal, N. Kejalakshmy, J. Chen, B. M. A. Rahman, and K. T. V. Grattan, "Golden spiral photonic crystal fiber: Polarization and dispersion properties," *Opt. Lett.*, vol. 33, no. 22, pp. 2716–2718, Nov. 2008.

[22] A. Agrawal, N. Kejalakshmy, B. M. A. Rahman, and K. T. V. Grattan, "Polarization and dispersion properties of elliptical hole golden spiral photonic crystal fiber," *Appl. Phys. B*, vol. 99, no. 4, pp. 717–726, 2010.

[23] S. M. A. Razzak and Y. Namihira, "Tailoring dispersion and confinement losses of photonic crystal fibers using hybrid cladding," *J. Lightw. Technol.*, vol. 26, no. 13, pp. 1909–1914, Jul. 2008.

[24] N. A. Mortensen and J. R. Folkenberg, "Low-loss criterion and effective area considerations for photonic crystal fibres," *J. Opt. A: Pure Appl. Opt.*, vol. 5, pp. 163–167, 2003.

[25] L. Xiao, W. Jin, and M. S. Demokan, "Fusion splicing small-core photonic crystal fibers and single-mode fibers by repeated arc discharges," *Opt. Lett.*, vol. 32, no. 2, pp. 115–117, 2007.

Md. Asiful Islam received the B.Sc. Eng. degree in electrical and electronic engineering from the Bangladesh University of Engineering and technology, Dhaka, Bangladesh, in 2009

He is currently a Lecturer at the Bangladesh University of Engineering and technology. His current research interests include finite-element modeling of photonic devices.

M. Shah Alam (SM'04) received the B.Sc. Eng., M.Sc. Eng., and the Ph.D. degrees in electrical and electronic engineering in 1989, 1994, and 1997, respectively. He received the Japanese Government Scholarship from April 1991 to March 1997 for pursuing his graduate studies, and received the Ph.D. degree from Hokkaido University, Sapporo, Japan.

In 1997, he was a Visiting Researcher in Electrotechnical Laboratory, Tsukuba, Japan. In 1998, he became a Lecturer in the Department of Electrical and Electronic Engineering, Bangladesh University of Engineering and Technology (BUET), Dhaka, Bangladesh, where he is currently a Professor. During 2003–2004, he was on postdoctoral study leave from BUET and worked as a Research Fellow with the Photonics Research Group in City University London, London, U.K. His current research interests include optical fibers, photonic crystal fibers, nonlinear properties in fibers, electro-optic modulators, the application of numerical techniques to guided wave photonics problems, and microwave integrated circuits.

Dr. Alam is a member of the Bangladesh Computer society and the Institution of Engineers, Bangladesh.